HHS Public Access

Author manuscript

J Physiol. Author manuscript; available in PMC 2022 January 19.

Published in final edited form as:

J Physiol. 2020 July ; 598(13): 2669–2683. doi:10.1113/JP279595.

Infiltration of intramuscular adipose tissue impairs skeletal muscle contraction

Nicole K. Biltz[1], **Kelsey H. Collins**[2,3], **Karen C. Shen**[1], **Kendall Schwartz**[4], **Charles A. Harris**[5], **Gretchen A. Meyer**[1,2,6]

[1]Program in Physical Therapy, Washington University, St. Louis, MO

[2]Department of Orthopaedic Surgery, Washington University, St. Louis, MO

[3]Shriners Hospitals for Children, St. Louis, MO

[4]Department of Biology, Washington University, St. Louis, MO

[5]Department of Medicine, Division of Endocrinology, Metabolism and Lipid Research, Washington University, St. Louis, MO

[6]Departments of Neurology and Biomedical Engineering, Washington University, St. Louis, MO

Abstract

Intramuscular adipose tissue (IMAT) is associated with deficits in strength and physical function across a wide array of conditions, from injury to ageing to metabolic disease. Due to the diverse aetiologies of the primary disorders involving IMAT and the strength of the associations, it has long been proposed that IMAT directly contributes to this muscle dysfunction. However, infiltration of IMAT and reduced strength could both be driven by muscle disuse, injury and systemic disease, making IMAT simply an 'innocent bystander.' Here, we utilize novel mouse models to evaluate the direct effect of IMAT on muscle contraction. First, we utilize intramuscular glycerol injection in wild-type mice to evaluate IMAT in the absence of systemic disease. In this model we find that, in isolation from the neuromuscular and circulatory systems, there remains a muscle-intrinsic association between increased IMAT volume and decreased contractile tension ($r^2 > 0.5$, $P < 0.01$) that cannot be explained by reduction in contractile material. Second, we utilize a lipodystrophic mouse model which cannot generate adipocytes to 'rescue' the deficits. We demonstrate that without IMAT infiltration, glycerol treatment does not reduce contractile force ($P > 0.8$). Taken together, this indicates that IMAT is not an inert feature of muscle pathology

Corresponding author G. A. Meyer: Program in Physical Therapy, Washington University in St. Louis, 4444 Forest Park Blvd, St. Louis, MO 63108. meyerg@wustl.edu.

Author contributions

This work was performed in the laboratory of GAM. The study was conceived and designed by NKB and GAM. Data were acquired, analysed and interpreted by NKB, KHC, KCS, KS, CAH and GAM. The manuscript was drafted by GAM and revised critically for important intellectual content by NKB, KHC, KCS, KS and CAH. All authors approved the final version of the manuscript and agree to be accountable for all aspects of the work.

Competing interests

The authors have no conflicts of interest to disclose.

Supporting information

Additional supporting information may be found online in the Supporting Information section at the end of the article.

but rather has a direct impact on muscle contraction. This finding suggests that novel strategies targeting IMAT may improve muscle strength and function in a number of populations.

Keywords

fat infiltration; IMAT; intermuscular adipose; muscle contraction

Introduction

An ectopic depot of adipose tissue develops in skeletal muscle in response to a variety of pathological conditions. These conditions encompass diverse aetiologies from orthopaedic injury (e.g. chronic rotator cuff tear, whiplash (Goutallier et al. 1994; Elliott et al. 2006)) to metabolic dysfunction (e.g. diabetes, renal disease (Goodpaster et al. 2003; Cheema et al. 2010)) to decreased loading (e.g. inactivity, spaceflight (Leskinen et al. 2013; Burkhart et al. 2019)). While no single causative factor has emerged across these disparate conditions, studies consistently find a common result – increased intramuscular adipose tissue (IMAT) is associated with decreased muscle strength and functional performance (Goodpaster et al. 2001; Gerber et al. 2007; Hilton et al. 2008; Buford et al. 2012; Tuttle et al. 2012; Khoja et al. 2018).

Logically, this is a predictable result. As non-contractile IMAT replaces an increasingly larger fraction of the muscle, contractile force will correspondingly decrease. However, evidence suggests that the role of IMAT in muscle contraction may be more complex than simple fatty replacement. Several clinical studies have found IMAT infiltration and decreased lean (IMAT-free) area to be de-coupled (Manini et al. 2007; Freda et al. 2008; Barry et al. 2013), suggesting that IMAT infiltration is not driven entirely by loss of contractile material. Furthermore, studies using detailed image segmentation to sub-divide IMAT and muscle ‘compartments’ have found that an association between IMAT quantity and strength persists per unit lean area (Manini et al. 2007; Delmonico et al. 2009; Marcus et al. 2013). These findings have led to speculation that IMAT could locally impair contraction in neighbouring myofibres. Hypothesized mechanisms include limiting neuromuscular activation (Yoshida et al. 2012), impeding muscle blood flow (Yim et al. 2007) and local secretion of pro-inflammatory adipokines (Manini et al. 2007; Marcus et al. 2010; Kelley & Goodpaster, 2015). However, in clinical studies these remain speculative as the injury, complex systemic disease and altered loading that drive IMAT infiltration also frequently affect neuromuscular performance, vascular perfusion and circulating levels of adipokines.

Animal studies are ideally poised to address such questions of mechanism; however, few have quantified both IMAT infiltration and muscle function. Of the studies that have noted an association between IMAT and decreased contractile force (Fukada et al. 2010; Meyer et al. 2011; Buras et al. 2019), all have been in chronic injury or disease models plagued by the same confounding factors as the aforementioned clinical studies. Recent work probing the mechanisms underlying IMAT development has avoided confounders associated with chronic injury and systemic disease by utilizing an intramuscular injection

of glycerol solution to induce IMAT infiltration with acute regeneration (reviewed in Mahdy (2018)). However, the functional consequences of persistent IMAT following resolution of regeneration have not been investigated. Thus, it remains unknown whether IMAT is associated with contractile deficits in the absence of injury and confounders of chronic and systemic disease and if so, if this relationship is causative.

In this work, we describe the relationship between IMAT and muscle contraction in a mouse model of glycerol injection. We utilize precision tools to quantify contractile performance and IMAT infiltration in the same muscles to determine salient predictive parameters. Finally, utilizing a constitutive transgenic lipodystrophic mouse model lacking all adipocytes, we investigate the causative role of IMAT in impaired muscle contraction. We hypothesize that IMAT directly impedes peak force production in muscle.

Methods

Ethical approval

All procedures were performed in accordance with the National Institutes of Health's Guide for the Use and Care of Laboratory Animals and were approved by the Animal Studies Committee of the Washington University School of Medicine (IACUC 20170267). The investigators understand the ethical principles under which the journal operates and confirm that this work complies with the animal ethics checklist.

Experimental design

Experiments were performed on 11–14-week-old male and female C57BL/6J mice (Jackson Laboratory, Bar Harbor, ME) and lipodystrophic (LD) mice (generated as previously described by Wu et al. 2018). Briefly, LD mice were created by crossing adiponectin-Cre mice with homozygous lox-stop-lox-ROSA-diphtheria toxin A mice, both on the C57BL/6J background. Mice with both Cre and diphtheria toxin transgenes lack mature adipocytes of any kind. All mice were 22–40 g in weight, and allowed free cage activity and *ad libitum* access to food and water. C57BL/6J mice were housed in standard 22°C conditions while LD mice and littermate wild-type (WT) controls were housed in thermoneutrality at 30°C. All experimental mice had glycerol injections to the mid-belly of one extensor digitorum longus (EDL) muscle to induce regeneration with infiltration of IMAT. The contralateral EDL was either injected with saline or cardiotoxin. Glycerol and cardiotoxin both provoke muscle regeneration by inducing myofibre necrosis, but glycerol treatment is reported to result in greater IMAT deposition (Mahdy et al. 2015) and thus cardiotoxin treatment was included to control for the effects of regeneration alone. A total of 92 mice were used in this study with a group size of 6–8 as indicated per measure.

Intramuscular injection

Mice were continuously anaesthetized with 2% inhaled isoflurane at 2 l min^{-1}. The depth of anaesthesia was assessed by toe pinch and ventilation rate. Hindlimbs were shaved and sterilized bilaterally with betadine. A 2–3 mm incision was made through the skin over the lateral aspect of each hindlimb exposing the distal-lateral quarter of the tibialis anterior muscle. The tibialis anterior was gently lifted to expose the belly of the EDL. 10

μl of either glycerol (50% v/v; Sigma Aldrich, St. Louis, MO), cardiotoxin (10 μM; *Naja mossambica mossambica*, Sigma Aldrich, St. Louis, MO) or sterile saline was then injected into the mid-belly of the EDL with a 29.5 gauge insulin syringe. Skin incisions were closed with suture glue and mice were given 5 mg kg^{-1} meloxicam via subcutaneous injection immediately following closure and again 24 h later for post-surgical analgesia. Mice were allowed free cage activity and were monitored daily for 72 h for signs of pain, distress and infection. No complications arose as a result of this procedure.

14 or 21 days following intramuscular injections, mice were again anaesthetized and the 5th toe belly of the EDL muscle was dissected bilaterally for *ex vivo* contractile assessment as previously described in detail (Moorwood et al. 2013). Dissection was performed under anaesthesia to maintain viability of the muscles. During dissection, LD and littermate WT mice were inspected for the presence of epididymal and inguinal fat pads. All LD mice lacked these fat pads, consistent with their expected phenotype (Wu et al. 2018). Following this procedure, mice were killed under anaesthesia by cervical dislocation. A subset of 24 mice underwent preparation of muscles for histological analysis only and were killed under anaesthesia by cervical dislocation prior to muscle collection.

Isolated muscle contractile assessment

Following dissection, muscles were transferred to a specialized small intact muscle stimulation system (1500A, Aurora Scientific, Aurora, ON, Canada) where physiology tests were run by a researcher blinded to the treatment condition. Within this system, the muscle was immersed in a bath of mammalian Ringer solution maintained at 37°C. The muscle was secured in the chamber using 6-0 black-braided silk suture to fix the origin and insertion to a stationary beam and a dual model ergonometer (300C-LR, Aurora Scientific, Aurora, ON, Canada), respectively. Muscle activation was controlled with an electrical stimulator (701C, Aurora Scientific, Aurora, ON, Canada) via parallel platinum plate electrodes extending along the muscle. Fibre length was measured using a dissecting microscope fitted with an eyepiece micrometre scale reticule. Muscle length was set when passive force just exceeded transducer noise (slack length). Optimal muscle length was then determined by incrementally increasing muscle length from slack by 10% of slack fibre length until the muscle isometric twitch force began to plateau, at which point length was further increased in increments of 5% slack length until isometric tetanic tension plateaued. At optimum length, force was recorded during a twitch contraction and isometric tetanic contraction (300 ms train of 0.3 ms pulses at 225 Hz). Fatigue was evaluated with repeated isometric tetanic contractions every 30 s until force dropped below 50% of peak. At this point, the muscle was cut from the sutures and weighed. This weight along with peak fibre length and muscle density (1.056 g/cm^3) was used to calculate the physiological cross-sectional area (PCSA) of the muscle. Muscle PCSA was adjusted for the measured volume of IMAT to account for the area occupied by non-contractile adipocytes and was then used to convert raw force to specific force (tension). The experiment was synchronized and recorded by a custom LabView (National Instruments) acquisition program and analysed using Matlab (Mathworks).

Five metrics of muscle contractile performance were quantified from this testing: 1) Peak twitch tension (Twitch Ten.) – peak of the force recording during the twitch contraction, normalized to adjusted PCSA; 2) Peak tetanic tension (Tetanic Ten.) – peak of the force recording during the tetanic contraction, normalized to adjusted PCSA; 3) Time to peak tension – the time between the initiation of force rise and peak during the twitch contraction; 4) Half-relaxation time – half the time between force peak and return to baseline during the twitch contraction; 5) Time to fatigue – time for the tetanic tension to fall below 50% of the peak value during the fatigue test.

Permeabilized fibre contractile assessment

Following contractile assessment, a subset of muscles were placed in a 0.5% w/v solution of Brij 58 (Sigma Aldrich, St. Louis, MO) for permeabilization and isolated fibre contractile testing as previously described in detail (Roche et al. 2015). Briefly, muscles were agitated in Brij 58 for 30 m before being stored at −20°C in a glycerinated storage solution. On the day of testing, individual fibres were teased from muscles in a relaxing solution and mounted in a permeabilized fibre stimulation system (1400A; Aurora Scientific, Aurora, ON, Canada). Fibre ends were affixed with 10-0 nylon suture to a force transducer (403A; Aurora Scientific, Aurora, ON, Canada) and a high-speed length controller (315C-I/322C; Aurora Scientific, Aurora, ON, Canada). Fibre length was increased until sarcomere length reached 2.5 μm as measured by the real-time Fourier transform of the banding pattern of the fibre on an inverted light microscope. Fibre diameter was measured on the light microscope image in three places along the length of the fibre and regeneration state was determined by the presence or absence of a chain of centrally localized nuclei. The fibre was then transferred to a pre-activating solution weakly buffered for calcium-enabling rapid activation when the fibre was finally moved to a 50 mM calcium-containing activating solution. Force rise upon activation was recorded and the fibre returned to a relaxing solution. Unless the fibre tore or slipped during testing, all measures are the average of three activation trials. Peak tension was normalized to fibre cross-sectional area (CSA) calculated from the average of the fibre diameter measurements. Only regenerated fibres were included in the final analysis of glycerol-treated muscles. Permeabilized fibre normalized tension is reported for each muscle as the average of 6–12 individual fibre tests. Composition of all solutions and detailed instructions for their preparation can be found in Roche et al. (2015).

Quantification of intramuscular adipose tissue

Following contractile assessment, a subset of muscles were placed in a 1% solution of sodium dodecyl sulfate (SDS; Sigma Aldrich, St. Louis, MO) for decellularization and IMAT quantification as previously described in detail (Biltz & Meyer, 2017). Briefly, muscles were incubated in SDS for 24 h, fixed in 3.7% formaldehyde for 48 h and incubated with the lipid soluble dye BODIPY (0.05 mg ml^{-1} BODIPY 493/503; Life Technologies, Carlsbad, CA) for 20 min. BODIPY signal was imaged through the muscle volume on an Olympus FV1200 scanning confocal microscope and individual adipocyte regions of interest (ROI) analysed in a semi-automated segmentation process based in ImageJ (NIH, Bethesda, MD). Following confocal imaging, muscles were stained with Oil Red O (ORO; Sigma Aldrich, St. Louis, MO) for visualization of spatial IMAT distribution and lipid quantification via alcohol extraction. Muscles from lipodystrophic and littermate control

mice were only stained with ORO and lipid volume was predicted from the optical density of the alcohol-extracted solution as previously described (Biltz & Meyer, 2017).

Five metrics of IMAT were quantified from confocal imaging: 1) Total lipid volume (Lipid Vol.) – sum of individual ROI volumes; 2) Relative lipid volume (Red. Lipid Vol.) – total lipid volume divided by total muscle volume; 3) Total number of adipocytes (Adipo. Count) – the number of identified ROIs; 4) Average adipocyte volume (Avg. Adipo. Vol.) – the average volume of the ROIs; 5) Nearest neighbour index – the average nearest neighbour Euclidian distance for each ROI divided by the average nearest neighbour distance in a hypothetical random distribution.

Histological analyses

Muscles for histological analysis were embedded in gastrocnemius muscle and flash frozen in liquid nitrogen-cooled isopentane as previously described (Biltz & Meyer, 2017). Muscles were cut at the mid-belly in 10 μm axial sections on a cryostat (Leica Biosystems, Wetzlar, Germany). Sections were stained with haematoxylin and eosin (H&E) to visualize tissue morphology, Picrosirius red to quantify collagen accumulation, and immunostained against myosin heavy chain isoforms (type I, type IIa, type IIx, type IIb and embryonic; BA-F8, SC-71, 6H1 and BF-45, respectively, Developmental Studies Hybridoma Bank, Iowa City, IA) and against laminin (ab11575; Abcam, Cambridge, UK) to quantify fibre types and areas and against PDGFRα (AF1062; R&D Systems, Minneapolis, MN) to quantify fibro/adipogenic progenitor cells (FAPs). The collagen area fraction was computed from one Picrosirius red stained 10× image that covered greater than 75% of the muscle CSA. Images were thresholded in ImageJ using the automated IsoData algorithm and the red-positive area was divided by the total area for an area fraction. Fibre types were identified on two non-overlapping 10× images that combined covered greater than 95% of the muscle CSA. Fibre counts for each type were divided by the total fibre number using a semi-automated ImageJ macro using the automated Huang threshold and particle analyser. Fibre areas were averaged from two non-overlapping laminin stained 20× images that combined covered greater than 75% of the muscle CSA. Fibre areas were detected with a custom ImageJ macro using the automated Huang threshold and particle analyser. Regions of interest with a circularity of less than 0.5 were excluded as being out of the axial plane of that fibre and only regenerated fibres, indicated by the presence of a centrally placed nucleus (Meyer, 2018), were included in the final analysis of glycerol-treated muscles. FAPs were identified by co-localization of PDGFRα and DAPI in the interstitial space as previously described (Bryniarski & Meyer, 2019).

Statistical analyses

Group sizes were selected based on a power analysis using existing contractile data from C57BL/6J male mouse EDL muscles and permeabilized fibres to estimate experimental variance and an anticipated effect size of 0.25.

Grouped data were analysed by two-way analysis of variance (ANOVA), with paired measurements between legs within a mouse, with the exception of time course data which was analysed by three-way ANOVA to assess time × sex × treatment interactions.

Bonferroni and Sidak multiple comparison tests were used to compare individual groups within the two- and three-way ANOVAs, respectively. A stepwise multilinear regression model was used to model the ability of IMAT metrics to predict contractile metrics. Linear regressions were performed between sets of independent variables to evaluate individual predictive abilities. Analyses of co-variance were run to determine significant deviations in linear relationships between treatments. All statistical analyses were run with Graphpad Prism (San Diego, CA), with the exception of the multilinear regression models which were run with Matlab (Natick, MA). All reported and plotted data are means ± standard deviation.

Results

Glycerol injection induces IMAT infiltration and contractile deficits

Consistent with previous reports (Pisani et al. 2010; Mahdy et al. 2015), injection of glycerol resulted in significant increases in IMAT (Fig. 1). Total volume of IMAT lipid (Fig. 1B), volume relative to muscle volume (Fig. 1C) and total number of adipocytes (Fig. 1D) were significantly increased in glycerol-treated muscles compared with contralateral saline treatment (main effect of treatment $P < 0.0005$ by two-way ANOVA). Post-test analysis found significant increases in both males and females across all three measures. The average volume of individual adipocytes was not different between treatments or sexes (Fig. 1E). However, there was a main effect of treatment ($P < 0.05$) in adipocyte spatial clustering (nearest neighbour index) with significant increases in both males and females, indicating a generally more dispersed distribution of adipocytes following glycerol treatment. Overall, these data indicate glycerol treatment increases the quantity and dispersion of IMAT adipocytes in muscle.

In addition to IMAT infiltration, glycerol injection induces transient muscle regeneration with initial reductions in muscle mass, fibre size and contractile tension that recover over time (Mahdy et al. 2015). At 21 days post-injection, the PCSA of glycerol-treated muscles returned to control values in both sexes (Fig. 2A). However, peak tension in both twitch (Fig. 2B) and tetanic (Fig. 2C) contractions remained significantly depressed (main effect of treatment $P < 0.005$ by two-way ANOVA). Post-test analysis found significantly lower tension in both males and females. Importantly, the normalization of peak twitch and tetanic tensions is to an adjusted PCSA which subtracts the lipid volume from the total muscle volume, thus representing only contractile material. Thus, the deficit in tension cannot be explained by replacement of contractile material with IMAT. Measures of calcium handling (time to peak tension and half-relaxation time) were not different between treatments or sexes (Fig. 2D and E, respectively). Similarly, there was no difference in time to fatigue between treatments or sexes (Fig. 2F). Taken together, this suggests that glycerol treatment results in deficits in contractile force generation not originating in calcium-handling machinery (e.g. sarcoplasmic reticulum) or metabolic changes (e.g. fibre type).

A subset of glycerol-injected muscles was compared with contralateral cardiotoxin-injected muscles as both treatments induce regeneration, but glycerol is reported to result in significantly more IMAT infiltration (Mahdy et al. 2015). However, in our hands, there was no difference between glycerol and cardiotoxin treatments in any IMAT or contractile metric.

IMAT infiltration is correlated with contractile tension deficits

To determine which, and to what degree, features of IMAT could explain contractile tension deficits, linear regression was performed pairwise between all metrics on the combined glycerol-injected dataset (those with saline and cardiotoxin-treated contralaterals). In male mice, the three measures of IMAT quantity (total IMAT lipid volume, relative lipid volume and total number of adipocytes) and average adipocyte volume were significantly negatively correlated with peak twitch and tetanic tensions (Fig. 3A). However, pairwise linear regression also indicated significant correlations between measures of IMAT quantity indicating that these are related variables. Thus, a stepwise regression was performed to determine the strongest independent predictor(s) of tension deficits. For both peak twitch and tetanic tension, total lipid volume was the only variable retained in the model, explaining 50% of the variance in twitch tension (Fig. 3B) and 85% of the variance in tetanic tension (Fig. 3C).

For female mice, peak twitch tension was not correlated with any IMAT measure, but peak tetanic tension and time to fatigue were significant negatively correlated with the three measures of IMAT quantity (Fig. 3D). Additionally, peak tetanic tension was significantly correlated with average adipocyte volume and time to fatigue was significantly correlated with the nearest neighbour index. Stepwise regression retained both total lipid volume and average adipocyte volume in the model as independent predictors to explain 90% of the variance in peak tetanic tension (Fig. 3E). The model for time to fatigue retained only total lipid volume, explaining a relatively modest 44% of the variance (Fig. 3F). Overall, this analysis indicates a strong correlation between the quantity of IMAT and peak contractile tension in male mice with a more complex relationship in female mice.

Interestingly, the linear relationships between peak tetanic tension and IMAT metrics identified by stepwise regression in glycerol-injected muscles were nearly identical to those in the cardiotoxin-injected muscles. Analysis of covariance (ANCOVA) found no significant differences in the regression lines fitting peak tetanic tension against total lipid volume in males ($P > 0.9$; GLY: −21588x + 303.65, CTX: −20738x + 297.46) or total lipid volume plus average adipocyte volume in females ($P > 0.5$; GLY: 1.00x + 375.0, CTX: 0.822x + 384.6). This suggests that the relationship between IMAT infiltration and contractile tension deficits is likely independent of the initiating toxin.

Glycerol-treated muscles exhibit fibrosis and reduced fibre cross-sectional area

Although we observed strong relationships between measures of IMAT infiltration and contractile function, these relationships are correlative. Other models of toxin-induced regeneration have noted associations between collagen deposition (fibrosis) and reduced fibre CSA and reduced contractile-specific tension (Mahdy et al. 2015). To address these confounding changes in our model, we assessed collagen content by Picrosirius red staining (Fig. 4A, centre column) and regenerated fibre area by laminin staining (Fig. 4A right column). We observed significantly increased collagen content at 21 days following glycerol treatment (main effect of treatment $P < 0.0001$ by two-way ANOVA). Post-test analysis found this increase to be significant for both males and females (Fig. 4B), suggesting a fibrotic response to glycerol treatment in both sexes. Regenerated fibre CSA was

significantly reduced at 21 days post-glycerol treatment in male muscle only (Fig. 4C). Two-way ANOVA found significant main effects of treatment ($p = 0.03$) and sex ($p = 0.0001$) with no significant interaction. This suggests that regenerated fibres may remain in an immature state in glycerol-treated male muscle. We also investigated the possibility that glycerol treatment induces a fibre-type shift, specifically toward immature and slow isoforms of myosin heavy chain, which could impact contractile function. However, no significant difference between glycerol- and saline-treated muscles was observed in either sex (Fig. 4D and E).

Isolated fibres do not exhibit a contractile deficit at 21 days post-glycerol treatment

To further explore the intrinsic capacity for force production in regenerated fibres, we tested both intact muscles and permeabilized regenerated fibres at 14 and 21 days post-glycerol treatment. If the contractile tension deficit in intact muscles was due to immature or disrupted sarcomeres in regenerated fibres, both muscles and fibres would exhibit a similar deficit in contraction. Peak tetanic tension of intact muscles is significantly reduced at both time points (Fig. 5A), although the deficit is smaller at day 21 than day 14 post-treatment (main effect of treatment $P<0.0001$, treatment–time interaction $P<0.05$ by three-way ANOVA). This reflects a partial recovery of contractile tension as muscle regeneration advances and sarcomere structure matures. In contrast, isolated permeabilized regenerated fibres only exhibit a significant contractile deficit at day 14 in male muscle (Fig. 5B). At day 21, both male and female glycerol-treated regenerated fibres have fully recovered peak tension (main effect of treatment $P < 0.01$, treatment–time interaction $P < 0.05$ by three-way ANOVA). Taken together, these data suggest that the deficit in peak tetanic tension in intact muscles at day 21 post-glycerol treatment is not due to the intrinsic structure of regenerated sarcomeres.

Glycerol-treated muscle from lipodystrophic mice exhibits neither IMAT infiltration nor contractile deficits

To further explore the causality of the relationship between IMAT infiltration and contractile function, we utilized male lipodystrophic (LD) mice which express diphtheria toxin under control of the adiponectin promoter and thus develop no adipocytes (Wu et al. 2018). Glycerol treatment to these muscles induced a similar increase in the undifferentiated FAP population (Fig 6A and B), but induced no IMAT infiltration (Fig. 6C and D). Interestingly, while WT littermate muscles again exhibited a significant deficit in peak tetanic tension with glycerol treatment, LD muscles did not (Fig. 6E). Two-way ANOVA found a significant treatment–genotype interaction in this measure ($p=0.02$), suggesting that the treatment affected the genotypes differently. Importantly, glycerol-treated LD muscles exhibit similarly increased collagen content (Fig. 6F centre column, Fig. 6G) and reduced fibre CSA (Fig. 6F right column, Fig. 6H) as WT littermates, with no treatment–genotype interactions by two-way ANOVA and exhibit no shift in fibre type distribution with glycerol treatment (Type 2b: SAL: 87.54 ± 4.43%, GLY: 88.31 ± 5.34%; Type 2x: SAL: 8.16 ± 3.66%, GLY: 6.38 ± 2.59%; Type 2a: SAL: 4.02 ± 0.99%, GLY: 5.14 ± 4.13%; Type 1: SAL: 0.28 ± 0.25%, GLY: 0.17 ± 0.32%). Taken together these data demonstrate a causal link between IMAT infiltration and contractile force deficits in glycerol-treated muscle.

Discussion

In this study, we establish an independent and causal link between increased IMAT infiltration and deficits in muscle contraction. Utilizing an intramuscular glycerol injection model, we describe a significant deficit in peak tetanic tension in WT mice that is strongly associated with IMAT quantity and is absent in lipodystrophic (LD) mice with the same experimental treatment but no IMAT infiltration. This finding indicates that IMAT is not an inert player in muscle injury and disease, but instead has an independent impact on muscle contraction. The direct link between IMAT and muscle weakness shown here represents foundational information from which investigations into novel therapeutic strategies can be launched.

To our knowledge, this is the first study to de-couple the drivers of IMAT formation from the effects of IMAT itself. Numerous clinical studies (Goodpaster et al. 2001; Gerber et al. 2007; Hilton et al. 2008; Buford et al. 2012; Tuttle et al. 2012; Khoja et al. 2018) and a few animal investigations (Fukada et al. 2010; Meyer et al. 2011; Buras et al. 2019) have documented correlations between IMAT quantity and muscle function, but these have all been in the context of chronic injury, systemic disease, altered loading or genetic myopathy that likely include direct effects on muscle contraction. In this study, we avoid most of these chronic confounders by employing local intramuscular glycerol injection which induces transient regeneration with IMAT deposition (Mahdy, 2018). While the early phases of regeneration are characterized by necrosis, inflammation and nascent muscle formation, these resolve after about 7 days and later stages primarily involve fibre hypertrophy (Lukjanenko et al. 2013; Mahdy et al. 2016). We chose to perform experiments at day 21 as it is the latest time point characterized in this model (Lukjanenko et al. 2013); however, our data suggest that fibre hypertrophy is not complete at this time point (Fig. 4C), despite recovery of muscle PCSA (Fig. 2A). If these smaller fibres lacked mature contractile properties, this could confound our findings as increased IMAT and immature fibres could be related to injection efficiency, rather than to each other. However, we find that isolated permeabilized fibres recover normal contractile tension by day 21 post-treatment (Fig. 5B). Furthermore, LD mice that do not develop IMAT have similar reductions in fibre CSA without concurrent reduction in peak tetanic tension (Fig. 5*C* and *F*). Together these data suggest that fibres have fully recovered mature contractile machinery by day 21 post-glycerol treatment despite ongoing hypertrophy.

Another confounding factor in the glycerol injection model is fibrosis. Fibrosis frequently accompanies IMAT infiltration in clinical conditions and animal models and is reported to be associated with deficits in muscle function (Valencia et al. 2017; Abramowitz et al. 2018; Buras et al. 2019). Similar to previous reports (Mahdy et al. 2015) we find increased extracellular matrix in glycerol-treated muscle (Fig. 4B). However, interestingly, we find a similar fibrotic increase in treated LD muscle which exhibits no contractile deficit (Fig. 5*C* and *E*), suggesting that this degree of fibrosis in the absence of IMAT infiltration is not sufficient to impair contraction. Though fibrosis has long been considered to negatively impact muscle contraction, our finding is in line with a handful of studies attempting to restore contractile function by resolving fibrosis, by a variety of mechanisms including inhibition of collagen gene expression and modulation of metalloproteases and TGF-β

signalling. The results of these studies have varied from partial improvement to worsened function (Huebner et al. 2008; Li et al. 2009; Gumucio et al. 2013). This may reflect the complex role of the extracellular matrix in muscle contraction, as it has both an important physiological function in force transmission and healing and a pathological role in the development of stiffness and contracture (Mann et al. 2011). It is possible that even at late stages of regeneration, increased collagen content is playing a physiological, rather than pathological, role – restoring structural integration and lateral force transmission.

We believe this work to also be the first report characterizing muscle regeneration in the absence of mature adipocytes. Two recent studies have used ablation models which drive diphtheria toxin under the control of other adipogenic regulatory genes (specifically peroxisome proliferator-activated receptor gamma (Pparg) and fatty acid binding protein-4 (Fabp4)) (Liu et al. 2012; Dammone et al. 2018). However, these genes are also expressed in undifferentiated progenitors of the stromovascular fraction (Shan et al. 2013). The so-called FAPs resident in the stromovascular fraction of muscle are believed to play an important role in supporting muscle regeneration (Joe et al. 2010; Heredia et al. 2013). In line with these findings, ablation of Pparg- and Fabp4-expressing cells impairs regeneration (Liu et al. 2012; Dammone et al. 2018). In contrast, we find that ablation of cells expressing adiponectin, which is localized to mature adipocytes (Berry & Rodeheffer, 2013), spares the undifferentiated FAP population and does not grossly impair regeneration (Fig. 6). A limitation to this model is that LD muscle has some degree of dysfunction at baseline with approximately 23% lower fibre CSA and 17% lower peak tetanic tension. However, the normalized regenerative response appears very similar to littermate WT controls in terms of fibrotic area (WT: 49.2%, LDL: 49.0%) and fibre CSA (WT: −20.0%, LD: −20.5%), with the notable exception of full recovery of peak tetanic tension in regenerated LD muscle. Thus, mature adipocytes do not appear to be necessary to mount a robust regenerative response in this model system. While LD muscle does not develop IMAT, it does accumulate intramyocellular lipid (IMCL). Reports on the impact of IMCL on muscle contraction are mixed, with some reporting an association with contractile deficit and some reporting an association with improved performance – the so-called ‘athlete’s paradox’ (Li et al. 2019). Qualitatively, LD EDL muscle exhibits only sporadic fibres with increased ORO-positive IMCL droplets in both saline and glycerol treatments. However, further detailed investigation is needed to eliminate IMCL as a driver of reduced tetanic tension in LD EDL muscle.

A number of clinical investigations have noted or suggested sex differences in the functional consequences of IMAT accumulation (Goodpaster et al. 2001; Guglielmi et al. 2014; Ofori et al. 2019). Thus, we investigated whether the influence of IMAT on muscle contraction might be sex-specific. None of the measures of IMAT infiltration had a significant main effect of sex or a significant sex–treatment interaction by two-way ANOVA, suggesting that IMAT infiltration was similar between sexes (Fig. 1). Contractile measures were also similar between males and females with only adjusted PCSA exhibiting a main effect of sex by two-way ANOVA and no measures with a significant sex–treatment interaction (Fig. 2). However, despite these similarities, regression of IMAT metrics against contractile metrics showed interesting sex specificity with IMAT predicting peak twitch tension only in males and time to fatigue only in females (Fig. 3). The full recovery of fibre CSA at

day 21 post-treatment (Fig. 4C) and of isolated permeabilized fibre peak tension at day 14 post-treatment (Fig. 5B) in females only suggests the possibility that females undergo a faster regenerative response in response to glycerol injection. Whether this or other global sex variations underlie the regression differences warrants further investigation. A limitation of the current study is that the link between IMAT and force deficits is explored in a predominantly fast-fibred muscle. Most clinical investigations are in mixed fibre type muscles and regional specificity of IMAT accumulation has been noted. Whether IMAT accumulation differs between predominately fast, mixed and slow muscles also warrants further investigation.

A causal link between IMAT and muscle strength deficits has been proposed in a number of studies (Manini et al. 2007; Yim et al. 2007; Marcus et al. 2010; Yoshida et al. 2012). Yoshida *et al.* proposed that IMAT around neuromuscular connections could impair the ability to activate muscle as IMAT was correlated with decreased central activation in older adults (Yoshida et al. 2012). Similarly, a few reports have suggested that IMAT around vessels could impede blood flow and oxygen delivery (Goodpaster et al. 2000; Yim et al. 2007). In this work, we are able to eliminate the effects of neuromuscular activation and blood-based oxygen delivery by measuring contraction *ex vivo*. In our testing paradigm, contraction is elicited through direct depolarization of muscle fibre membranes, circumventing the neuromuscular junction, and oxygen is delivered via diffusion in the bath of Ringer's solution. As we still find significant associations between IMAT and muscle contraction (Fig. 3), it is unlikely that the mechanism lies in acute impedance of neural or vascular structures. We are unable to eliminate long-term adaptations to the muscle fibres in response to *in vivo* impairments in innervation or blood flow. Given that isolated permeabilized muscle fibres exhibit no contractile deficit at day 21 post-treatment (Fig. 5B), adaptations in the sarcomere structure are unlikely. However, we are unable to eliminate the possibility that fibres with impaired sarcomere organization were excluded from testing due to structural failure.

The prevailing hypothesis for a direct impact of IMAT on muscle contraction is local release of pro-inflammatory adipokines (Manini et al. 2007; Marcus et al. 2010; Kelley & Goodpaster, 2015). Generally, expansion of ectopic adipose tissue outside of the subcutaneous depot (e.g. visceral, IMAT) is associated with an elevated circulating pro-inflammatory cytokine profile (Beasley et al. 2009). Further, *in vitro* studies demonstrate the capacity for adipokines to impact physiology at the level of the muscle cell (Takegahara et al. 2014) and our recent *in vivo* model confirms that adipokines can act on muscle at a local level via paracrine signalling (Bryniarski & Meyer, 2019). Intriguingly, both IMAT and the pro-inflammatory adipokine TNFα were found to be locally increased in the paretic leg of stroke survivors (Hafer-Macko et al. 2005), suggesting that the inflammatory milieu could be locally impacted by IMAT. TNFα has been shown to impair contractile force in isolated muscle fibres and fibre bundles (Hopkins, 1996; Reid et al. 2002). Importantly, this impairment persists during testing once the exposure had been removed and is not associated with altered calcium transients or overt catabolism (Reid et al. 2002). These findings align with the data presented here indicating no association of IMAT metrics with measures of calcium handling (Fig. 3) and no functional deficits in isolated permeabilized fibres at day 21 post-treatment (Fig. 5B). Further studies are needed to determine whether local secretion

of pro-inflammatory adipokines such as TNFα or another yet to be defined mechanism underlies the impairment of contractile function, but our work here, identifying a direct link with IMAT, is a positive step toward developing targeted therapies to improve strength and quality of life in the context of IMAT infiltration in a wide array of populations.

Supplementary Material

Refer to Web version on PubMed Central for supplementary material.

Funding

Funding for this work was provided by the Program in Physical Therapy at Washington University School of Medicine.

Data was acquired in part through the use of the Washington University Centre for Cellular Imaging (WUCCI) supported by Washington University School of Medicine, The Children's Discovery Institute of Washington University and St. Louis Children's Hospital (CDI-CORE-2015-505 and CDI-CORE-2019-813) and the Foundation for Barnes-Jewish Hospital (3770 and 4642). Additional data acquisition support was provided by the Nutrition and Obesity Research Centre (NIH P30 DK056341) and the Musculoskeletal Research Centre (NIH P30 AR074992).

Biography

Nicole Biltz is a physical therapist and board-certified clinical specialist in neurologic physical therapy. She received her doctorate in physical therapy (DPT) at Washington University in St. Louis, where she worked alongside Dr Gretchen Meyer in her lab studying integrative muscle physiology. As a physical therapist, Nicole provided a clinical perspective to this very important research identifying a possible interaction between intramuscular adipose tissue and muscle. In the future, Nicole aspires to acquire either a PhD or an EdD, and teach within a DPT programme, spreading the passion for both research and patient care.

Data availability statement

The data that support the findings of this study are available from the corresponding author upon reasonable request.

References

Abramowitz MK, Paredes W, Zhang K, Brightwell CR, Newsom JN, Kwon HJ, Custodio M, Buttar RS, Farooq H, Zaidi B, Pai R, Pessin JE, Hawkins M & Fry CS (2018). Skeletal muscle fibrosis is associated with decreased muscle inflammation and weakness in patients with chronic kidney disease. Am J Physiol Renal Physiol 315, F1658–F1669. [PubMed: 30280599]

Barry JJ, Lansdown DA, Cheung S, Feeley BT & Ma CB (2013). The relationship between tear severity, fatty infiltration, and muscle atrophy in the supraspinatus. J Shoulder Elbow Surg 22, 18–25. [PubMed: 22541866]

Beasley LE, Koster A, Newman AB, Javaid MK, Ferrucci L, Kritchevsky SB, Kuller LH, Pahor M, Schaap LA, Visser M, Rubin SM, Goodpaster BH & Harris TB & study HA (2009). Inflammation

and race and gender differences in computerized tomography-measured adipose depots. Obesity (Silver Spring) 17, 1062–1069. [PubMed: 19165157]

Berry R & Rodeheffer MS (2013). Characterization of the adipocyte cellular lineage in vivo. Nat Cell Biol 15, 302–308. [PubMed: 23434825]

Biltz NK & Meyer GA (2017). A novel method for the quantification of fatty infiltration in skeletal muscle. Skelet Muscle 7, 1.

Bryniarski AR & Meyer GA (2019). Brown Fat Promotes Muscle Growth During Regeneration. J Orthop Res 37, 1817–1826. [PubMed: 31042310]

Buford TW, Lott DJ, Marzetti E, Wohlgemuth SE, Vandenborne K, Pahor M, Leeuwenburgh C & Manini TM (2012). Age-related differences in lower extremity tissue compartments and associations with physical function in older adults. Exp Gerontol 47, 38–44. [PubMed: 22015325]

Buras ED, Converso-Baran K, Davis CS, Akama T, Hikage F, Michele DE, Brooks SV & Chun TH (2019). Fibro-Adipogenic Remodeling of the Diaphragm in Obesity-Associated Respiratory Dysfunction. Diabetes 68, 45–56. [PubMed: 30361289]

Burkhart K, Allaire B & Bouxsein ML (2019). Negative Effects of Long-duration Spaceflight on Paraspinal Muscle Morphology. Spine (Phila Pa 1976) 44, 879–886. [PubMed: 30624302]

Cheema B, Abas H, Smith B, O'Sullivan AJ, Chan M, Patwardhan A, Kelly J, Gillin A, Pang G, Lloyd B, Berger K, Baune BT & Singh MF (2010). Investigation of skeletal muscle quantity and quality in end-stage renal disease. Nephrology (Carlton) 15, 454–463. [PubMed: 20609098]

Dammone G, Karaz S, Lukjanenko L, Winkler C, Sizzano F, Jacot G, Migliavacca E, Palini A, Desvergne B, Gilardi F & Feige JN (2018). PPARγ Controls Ectopic Adipogenesis and Cross-Talks with Myogenesis During Skeletal Muscle Regeneration. Int J Mol Sci 19, 2044.

Delmonico MJ, Harris TB, Visser M, Park SW, Conroy MB, Velasquez-Mieyer P, Boudreau R, Manini TM, Nevitt M, Newman AB & Goodpaster BH & Health, Aging, and Body Composition Study (2009). Longitudinal study of muscle strength, quality, and adipose tissue infiltration. Am J Clin Nutr 90, 1579–1585. [PubMed: 19864405]

Elliott J, Jull G, Noteboom JT, Darnell R, Galloway G & Gibbon WW (2006). Fatty infiltration in the cervical extensor muscles in persistent whiplash-associated disorders: a magnetic resonance imaging analysis. Spine (Phila Pa 1976) 31, E847–855. [PubMed: 17047533]

Freda PU, Shen W, Heymsfield SB, Reyes-Vidal CM, Geer EB, Bruce JN & Gallagher D (2008). Lower visceral and subcutaneous but higher intermuscular adipose tissue depots in patients with growth hormone and insulin-like growth factor I excess due to acromegaly. J Clin Endocrinol Metab 93, 2334–2343. [PubMed: 18349062]

Fukada S, Morikawa D, Yamamoto Y, Yoshida T, Sumie N, Yamaguchi M, Ito T, Miyagoe-Suzuki Y, Takeda S, Tsujikawa K & Yamamoto H (2010). Genetic background affects properties of satellite cells and mdx phenotypes. Am J Pathol 176, 2414–2424. [PubMed: 20304955]

Gerber C, Schneeberger AG, Hoppeler H & Meyer DC (2007). Correlation of atrophy and fatty infiltration on strength and integrity of rotator cuff repairs: a study in thirteen patients. J Shoulder Elbow Surg 16, 691–696. [PubMed: 17931904]

Goodpaster BH, Carlson CL, Visser M, Kelley DE, Scherzinger A, Harris TB, Stamm E & Newman AB (2001). Attenuation of skeletal muscle and strength in the elderly: The Health ABC Study. J Appl Physiol (1985) 90, 2157–2165. [PubMed: 11356778]

Goodpaster BH, Krishnaswami S, Resnick H, Kelley DE, Haggerty C, Harris TB, Schwartz AV, Kritchevsky S & Newman AB (2003). Association between regional adipose tissue distribution and both type 2 diabetes and impaired glucose tolerance in elderly men and women. Diabetes Care 26, 372–379. [PubMed: 12547865]

Goodpaster BH, Thaete FL & Kelley DE (2000). Thigh adipose tissue distribution is associated with insulin resistance in obesity and in type 2 diabetes mellitus. Am J Clin Nutr 71, 885–892. [PubMed: 10731493]

Goutallier D, Postel JM, Bernageau J, Lavau L & Voisin MC (1994). Fatty muscle degeneration in cuff ruptures. Pre- and postoperative evaluation by CT scan. Clin Orthop Relat Res Jul;(304), 78–83. [PubMed: 8020238]

Guglielmi V, Maresca L, D'Adamo M, Di Roma M, Lanzillo C, Federici M, Lauro D, Preziosi P, Bellia A & Sbraccia P (2014). Age-related different relationships between ectopic adipose tissues and measures of central obesity in sedentary subjects. PLoS One 9, e103381. [PubMed: 25051047]

Gumucio JP, Flood MD, Phan AC, Brooks SV & Mendias CL (2013). Targeted inhibition of TGF-β results in an initial improvement but long-term deficit in force production after contraction-induced skeletal muscle injury. J Appl Physiol (1985) 115, 539–545. [PubMed: 23766498]

Hafer-Macko CE, Yu S, Ryan AS, Ivey FM & Macko RF (2005). Elevated tumor necrosis factor-alpha in skeletal muscle after stroke. Stroke 36, 2021–2023. [PubMed: 16109906]

Heredia JE, Mukundan L, Chen FM, Mueller AA, Deo RC, Locksley RM, Rando TA & Chawla A (2013). Type 2 innate signals stimulate fibro/adipogenic progenitors to facilitate muscle regeneration. Cell 153, 376–388. [PubMed: 23582327]

Hilton TN, Tuttle LJ, Bohnert KL, Mueller MJ & Sinacore DR (2008). Excessive adipose tissue infiltration in skeletal muscle in individuals with obesity, diabetes mellitus, and peripheral neuropathy: association with performance and function. Phys Ther 88, 1336–1344. [PubMed: 18801853]

Hopkins PM (1996). Human recombinant TNF alpha affects rat diaphragm muscle in vitro. Intensive Care Med 22, 359–362. [PubMed: 8708176]

Huebner KD, Jassal DS, Halevy O, Pines M & Anderson JE (2008). Functional resolution of fibrosis in mdx mouse dystrophic heart and skeletal muscle by halofuginone. Am J Physiol Heart Circ Physiol 294, H1550–1561. [PubMed: 18263710]

Joe AW, Yi L, Natarajan A, Le Grand F, So L, Wang J, Rudnicki MA & Rossi FM (2010). Muscle injury activates resident fibro/adipogenic progenitors that facilitate myogenesis. Nat Cell Biol 12, 153–163. [PubMed: 20081841]

Kelley DE & Goodpaster BH (2015). Stewing in not-so-good juices: interactions of skeletal muscle with adipose secretions. Diabetes 64, 3055–3057. [PubMed: 26294424]

Khoja SS, Moore CG, Goodpaster BH, Delitto A & Piva SR (2018). Skeletal muscle fat and its association with physical function in rheumatoid arthritis. Arthritis Care Res (Hoboken) 70, 333–342. [PubMed: 28482146]

Leskinen T, Sipilä S, Kaprio J, Kainulainen H, Alen M & Kujala UM (2013). Physically active vs. inactive lifestyle, muscle properties, and glucose homeostasis in middle-aged and older twins. Age (Dordr) 35, 1917–1926. [PubMed: 23124702]

Li H, Mittal A, Makonchuk DY, Bhatnagar S & Kumar A (2009). Matrix metalloproteinase-9 inhibition ameliorates pathogenesis and improves skeletal muscle regeneration in muscular dystrophy. Hum Mol Genet 18, 2584–2598. [PubMed: 19401296]

Li X, Li Z, Zhao M, Nie Y, Liu P, Zhu Y & Zhang X (2019). Skeletal muscle lipid droplets and the athlete's paradox. Cells 8, 249.

Liu W, Liu Y, Lai X & Kuang S (2012). Intramuscular adipose is derived from a non-Pax3 lineage and required for efficient regeneration of skeletal muscles. Dev Biol 361, 27–38. [PubMed: 22037676]

Lukjanenko L, Brachat S, Pierrel E, Lach-Trifilieff E & Feige JN (2013). Genomic profiling reveals that transient adipogenic activation is a hallmark of mouse models of skeletal muscle regeneration. PLoS One 8, e71084. [PubMed: 23976982]

Mahdy MA, Lei HY, Wakamatsu J, Hosaka YZ & Nishimura T (2015). Comparative study of muscle regeneration following cardiotoxin and glycerol injury. Ann Anat 202, 18–27. [PubMed: 26340019]

Mahdy MA, Warita K & Hosaka YZ (2016). Early ultrastructural events of skeletal muscle damage following cardiotoxin-induced injury and glycerol-induced injury. Micron 91, 29–40. [PubMed: 27710777]

Mahdy MAA (2018). Glycerol-induced injury as a new model of muscle regeneration. Cell Tissue Res 374, 233–241. [PubMed: 29754258]

Manini TM, Clark BC, Nalls MA, Goodpaster BH, Ploutz-Snyder LL & Harris TB (2007). Reduced physical activity increases intermuscular adipose tissue in healthy young adults. Am J Clin Nutr 85, 377–384. [PubMed: 17284732]

Mann CJ, Perdiguero E, Kharraz Y, Aguilar S, Pessina P, Serrano AL & Muñoz-Cánoves P (2011). Aberrant repair and fibrosis development in skeletal muscle. Skelet Muscle 1, 21. [PubMed: 21798099]

Marcus RL, Addison O, Kidde JP, Dibble LE & Lastayo PC (2010). Skeletal muscle fat infiltration: impact of age, inactivity, and exercise. J Nutr Health Aging 14, 362–366. [PubMed: 20424803]

Marcus RL, Addison O & LaStayo PC (2013). Intramuscular adipose tissue attenuates gains in muscle quality in older adults at high risk for falling. A brief report. J Nutr Health Aging 17, 215–218. [PubMed: 23459972]

Meyer DC, Gerber C, Von Rechenberg B, Wirth SH & Farshad M (2011). Amplitude and strength of muscle contraction are reduced in experimental tears of the rotator cuff. Am J Sports Med 39, 1456–1461. [PubMed: 21350068]

Meyer GA (2018). Evidence of induced muscle regeneration persists for years in the mouse. Muscle Nerve 58, 858–862. [PubMed: 30159908]

Moorwood C, Liu M, Tian Z & Barton ER (2013). Isometric and eccentric force generation assessment of skeletal muscles isolated from murine models of muscular dystrophies. J Vis Exp, Jan 31;(71), e50036. [PubMed: 23407283]

Ofori EK, Conde Alonso S, Correas-Gomez L, Carnero EA, Zwygart K, Hugues H, Bardy D, Hans D, Dwyer AA & Amati F (2019). Thigh and abdominal adipose tissue depot associations with testosterone levels in postmenopausal females. Clin Endocrinol (Oxf) 90, 433–439. [PubMed: 30575083]

Pisani DF, Bottema CD, Butori C, Dani C & Dechesne CA (2010). Mouse model of skeletal muscle adiposity: a glycerol treatment approach. Biochem Biophys Res Commun 396, 767–773. [PubMed: 20457129]

Reid MB, Lännergren J & Westerblad H (2002). Respiratory and limb muscle weakness induced by tumor necrosis factor-alpha: involvement of muscle myofilaments. Am J Respir Crit Care Med 166, 479–484. [PubMed: 12186824]

Roche SM, Gumucio JP, Brooks SV, Mendias CL & Claflin DR (2015). Measurement of Maximum Isometric Force Generated by Permeabilized Skeletal Muscle Fibers. J Vis Exp, e52695. [PubMed: 26131687]

Shan T, Liu W & Kuang S (2013). Fatty acid binding protein 4 expression marks a population of adipocyte progenitors in white and brown adipose tissues. FASEB J 27, 277–287. [PubMed: 23047894]

Takegahara Y, Yamanouchi K, Nakamura K, Nakano S & Nishihara M (2014). Myotube formation is affected by adipogenic lineage cells in a cell-to-cell contact-independent manner. Exp Cell Res 324, 105–114. [PubMed: 24720912]

Tuttle LJ, Sinacore DR & Mueller MJ (2012). Intermuscular adipose tissue is muscle specific and associated with poor functional performance. J Aging Res 2012, 172957. [PubMed: 22666591]

Valencia AP, Iyer SR, Spangenburg EE, Gilotra MN & Lovering RM (2017). Impaired contractile function of the supraspinatus in the acute period following a rotator cuff tear. BMC Musculoskelet Disord 18, 436. [PubMed: 29121906]

Wu X, Hutson I, Akk AM, Mascharak S, Pham CTN, Hourcade DE, Brown R, Atkinson JP & Harris CA (2018). Contribution of Adipose-Derived Factor D/Adipsin to Complement Alternative Pathway Activation: Lessons from Lipodystrophy. J Immunol 200, 2786–2797. [PubMed: 29531168]

Yim JE, Heshka S, Albu J, Heymsfield S, Kuznia P, Harris T & Gallagher D (2007). Intermuscular adipose tissue rivals visceral adipose tissue in independent associations with cardiovascular risk. Int J Obes (Lond) 31, 1400–1405. [PubMed: 17452994]

Yoshida Y, Marcus RL & Lastayo PC (2012). Intramuscular adipose tissue and central activation in older adults. Muscle Nerve 46, 813–816. [PubMed: 23055318]

Key points

- Muscle infiltration with adipose tissue (IMAT) is common and associated with loss of skeletal muscle strength and physical function across a diverse set of pathologies.
- Whether the association between IMAT and muscle weakness is causative or simply correlative remains an open question that needs to be addressed to effectively guide muscle strengthening interventions in people with increased IMAT.
- In the present studies, we demonstrate that IMAT deposition causes decreased muscle strength using mouse models.
- These findings indicate IMAT is a novel therapeutic target for muscle dysfunction.

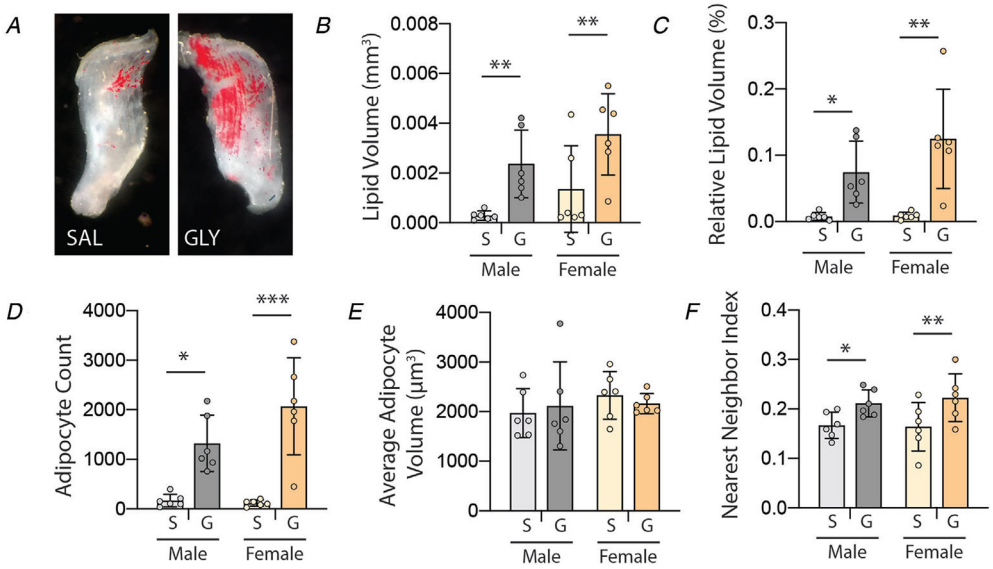

Figure 1. Intramuscular glycerol injection induces IMAT infiltration at 21 days post-treatment

A, Oil Red O staining of decellularized EDL muscle treated with saline (SAL) and glycerol (GLY) depicting increased quantity and dispersion of IMAT adipocytes (red) following glycerol treatment. *B–F*, quantification of IMAT infiltration metrics by confocal analysis as a function of treatment (S: saline, G: glycerol) and sex. Quantification confirms increased total and relative lipid volumes, total adipocyte count and nearest neighbour index (dispersion) with glycerol treatment in both sexes. $N = 6$, $^{*}P < 0.05$, $^{**}P < 0.01$, $^{***}P < 0.005$ by Bonferroni post-test on two-way ANOVA.

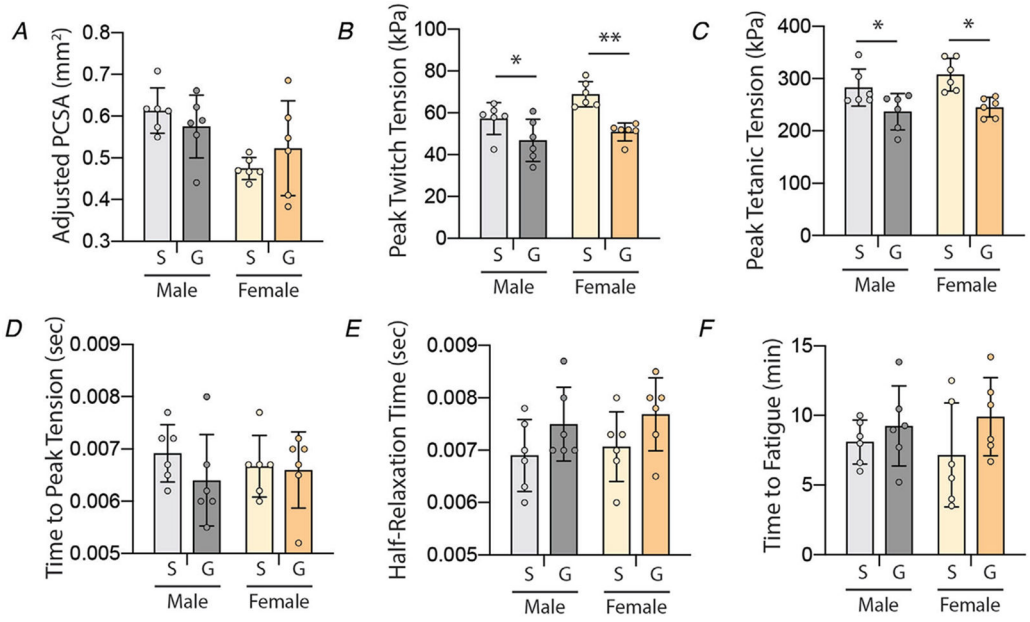

Figure 2. Intramuscular glycerol injection causes reductions in peak contractile tension at 21 days post-treatment

A, EDL physiological cross-sectional area (PCSA), adjusted for the quantity of IMAT, is not different between treatment groups (S: saline, G: glycerol). *B–C*, peak tension (normalized to adjusted PCSA) is reduced with glycerol treatment in both twitch and tetanic contractions in both sexes. *D–E*, measures of calcium handling – time to peak tension and half-relaxation time – are not affected by glycerol treatment. *F*, time to fatigue is not affected by glycerol treatment. $N = 6$; $*P < 0.05$, $**P < 0.01$ by Bonferroni post-test on two-way ANOVA.

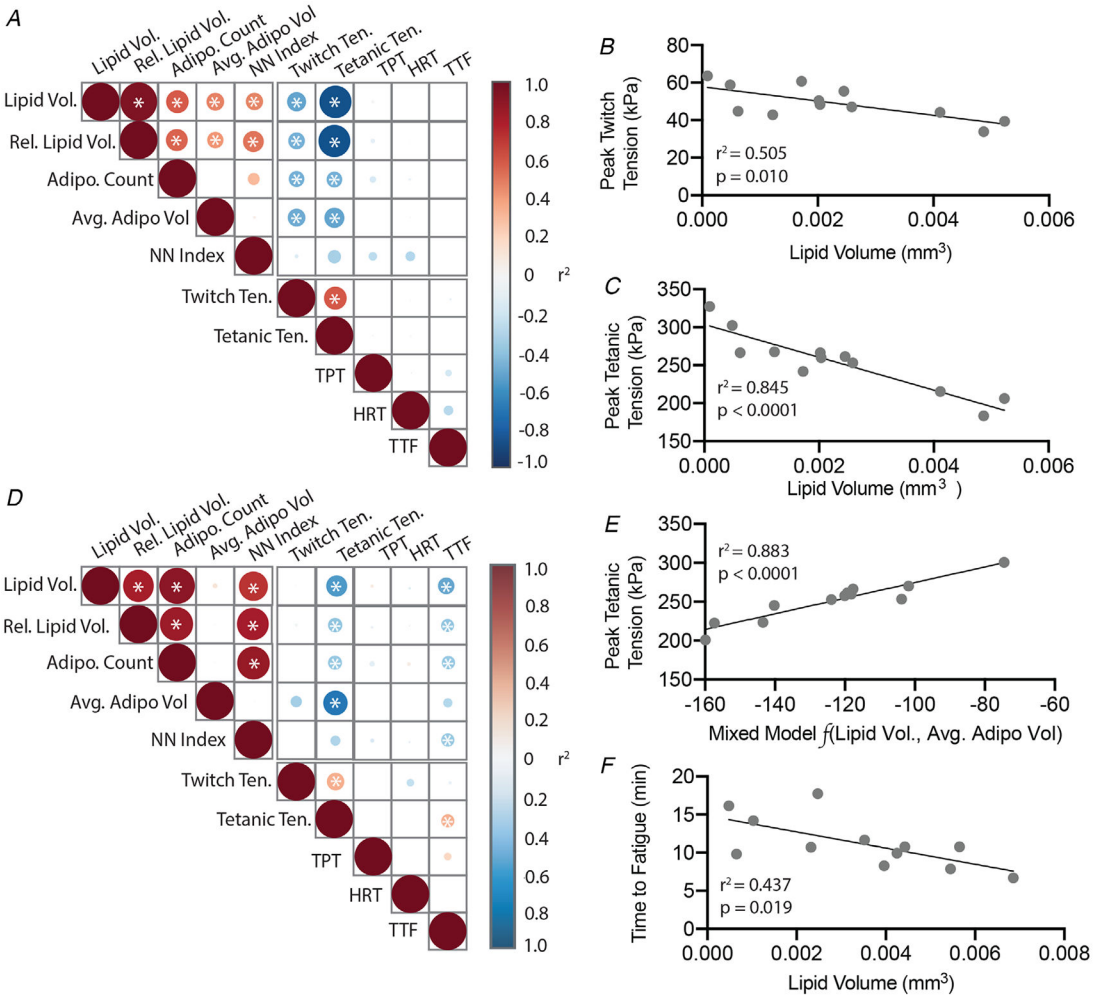

Figure 3. IMAT metrics are correlated with contractile deficits in male and female EDL muscles

A and *D*, pairwise regression matrices for male and female mice, respectively. The strength of individual correlations is indicated by the circle size and colour in each box with red and blue shades indicating positive and negative correlations, respectively. Internal asterisks denote significant relationships. *B–C*, linear regressions of peak twitch and tetanic tensions against lipid volume in male mice. Lipid volume was the strongest linear predictor of both tensions by stepwise multilinear regression. *E*, linear regression of peak tetanic tension against a linear combination of lipid volume and average adipocyte volume in female mice. Lipid volume and average adipocyte volume in linear combination were the strongest predictors of peak tetanic tension by stepwise multilinear regression. *F*, linear regressions of time to fatigue against lipid volume in female mice. Lipid volume was the strongest predictor of time to fatigue by stepwise multilinear regression. $N = 12$.

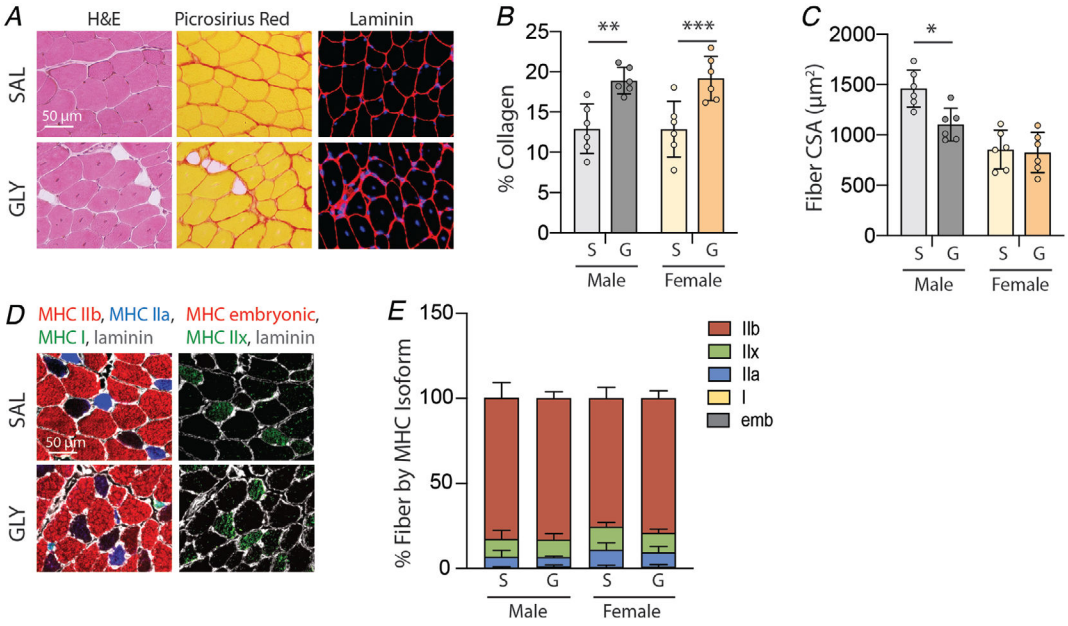

Figure 4. Intramuscular glycerol injection increases collagen content and decreases fibre area at 21 days post-treatment

A, representative images of saline- (SAL) and glycerol (GLY)-treated EDL sections stained with haematoxylin & eosin (H&E) to visualize tissue morphology, Picrosirius red to visualize collagen (red) and laminin to visualize fibre areas (red-rimmed areas). Note the appearance of intramuscular adipocytes (unstained areas) and centrally placed nuclei (blue in fibre centres) in GLY-treated muscles. *B*, quantification of Picrosirius red staining indicates increased collagen deposition with glycerol treatment (S: saline, G: glycerol) in both sexes. *C*, quantification of fibre cross-sectional area (CSA) on laminin-stained sections indicates decreased fibre CSA in glycerol-treated male muscle only. *D*, representative images of myosin heavy chain (MHC) isoform immunostaining to identify fibre types. *E*, quantification of MHC isoform distribution in stained sections reveals no significant shifts in fibre type distributions with glycerol treatment. $N = 6$; $^{*}P < 0.05$, $^{**}P < 0.01$, $^{***}P < 0.005$ by Bonferroni post-test on two-way ANOVA.

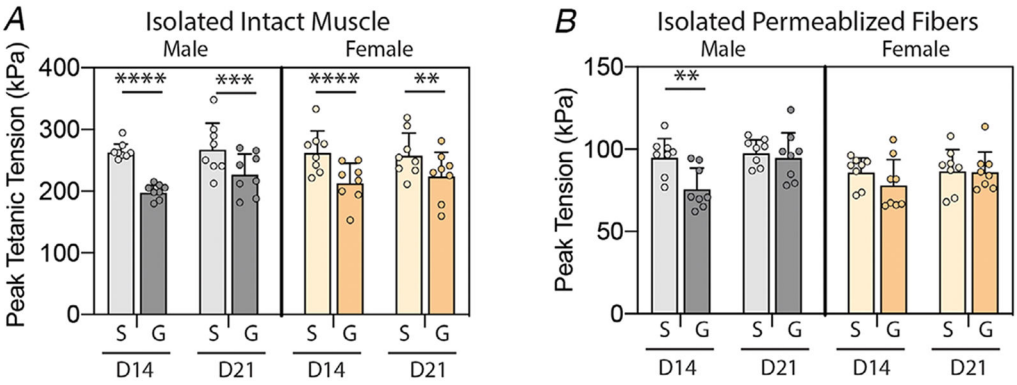

Figure 5. Intact muscles exhibit a residual contractile tension deficit at day 21 post-treatment while permeabilized fibres do not

A, peak tetanic tension measured in isolated EDL muscles at day 14 (D14) and day 21 (D21) post-treatment (S: saline, G: glycerol) in male and female mice. Glycerol injection reduces peak tetanic tension at both time points in both sexes. *B*, peak tension measured in permeabilized fibres isolated from muscles in the indicated groups in A. Glycerol injection reduces peak tension only in male mice and only at day 14. Full recovery of tension is seen in both sexes at day 21. $N = 8$; $^{**}P < 0.01$, $^{***}P < 0.005$, $^{****}P < 0.001$ by Sidak post-test on three-way ANOVA.

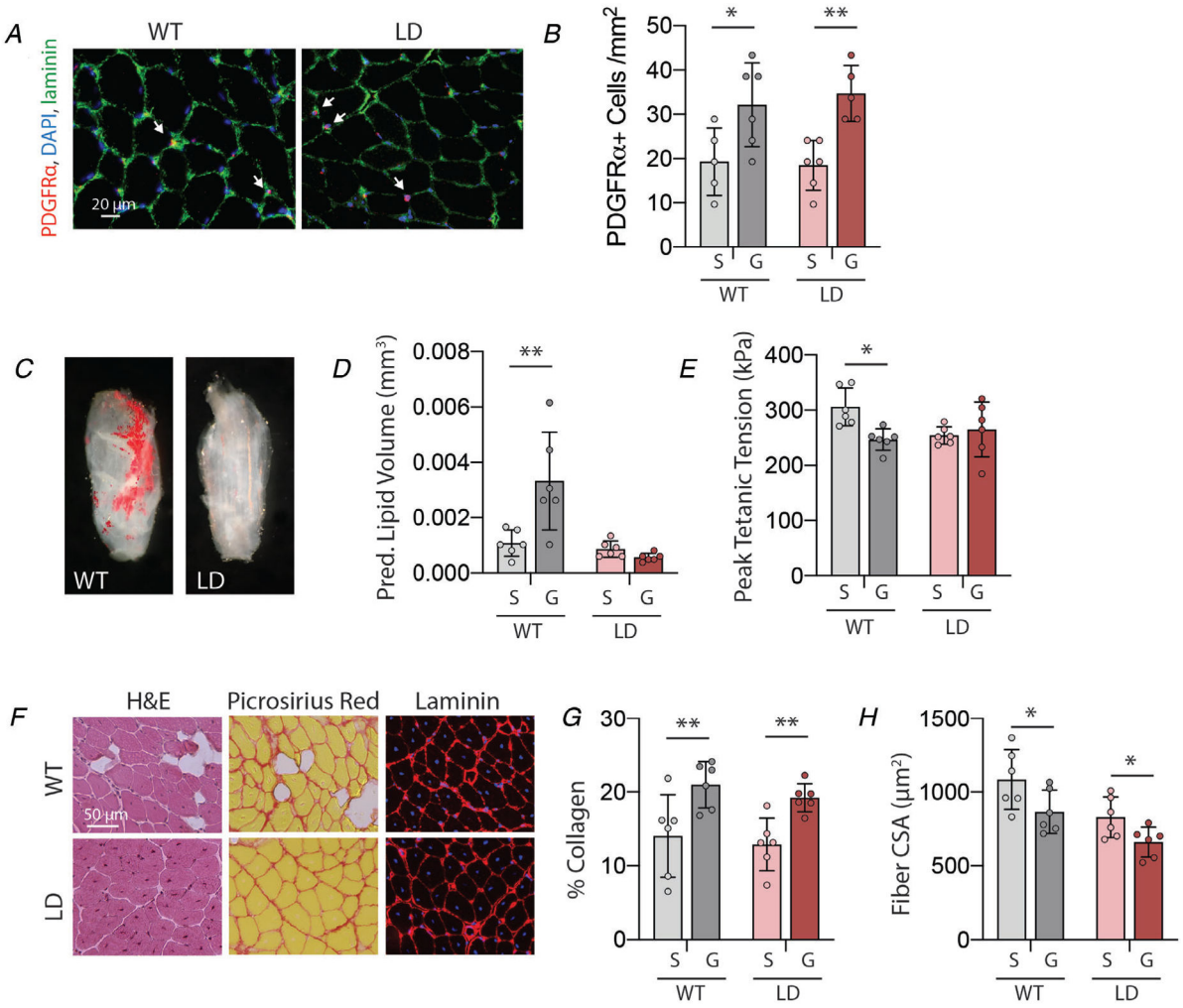

Figure 6. Lipodystrophic muscle develops neither IMAT nor a contractile deficit at day 21 post-glycerol treatment

A, representative images of PDGFR*α* immunostaining identifying fibro/adipogenic progeitors (FAPs). *B*, quantification of FAPs per unit area indicates an increase with glycerol (G) treatment compared with saline (S) in both wildtype (WT) and lipodystrophic (LD) genotypes. *C*, Oil Red O staining of decellularized male glycerol-treated EDL depicting absence of IMAT in lipodystrophic (LD) muscle compared with littermate wildtype (WT) controls. *D*, predicted lipid volume from Oil Red O extraction indicates a significant increase with glycerol treatment (S: saline, G: glycerol) in WT mice only. *E*, peak tetanic tension is significantly reduced with glycerol treatment in WT mice only. *F*, representative images of WT and LD glycerol-treated EDL sections stained with haematoxylin & eosin (H&E) to visualize tissue morphology, Picrosirius red to visualize collagen (red) and laminin to visualize fibre areas (red-rimmed areas). Note the appearance of intramuscular adipocytes (unstained areas) in WT only but centrally placed nuclei (blue in fibre centres) in both genotypes. *G*, quantification of Picrosirius red staining indicates increased collagen deposition with glycerol treatment in both genotypes. *H*, quantification of fibre cross-sectional area (CSA) on laminin-stained sections indicates decreased fibre CSA with

glycerol treatment in both genotypes. $N = 6$; $^{*}P < 0.05$, $^{**}P < 0.01$ by Bonferroni post-test on two-way ANOVA.